Chemical Synthesis

Research Article

Coke deposition mechanisms of propane dehydrogenation on different sites of Al$_2$O$_3$ supported PtSn catalysts

Jianhao Jiao[1,2], Ye Yang[2,*], Maojie Yuan[2], Xuqi Tang[2], Mengfan Shi[2], Kai He[1,2], Haijuan Zhang[2], Yanfeng Bi[2], Yucai Qin[2], Lijuan Song[1,2,*]

[1]College of Chemistry and Chemical Engineering, China University of Petroleum (East China), Qingdao 266555, Shandong, China.
[2]Key Laboratory of Petrochemical Catalytic Science and Technology, Liaoning Petrochemical University, Fushun 113001, Liaoning, China.

*****Correspondence to:** Dr. Ye Yang, Prof. Lijuan Song, Key Laboratory of Petrochemical Catalytic Science and Technology, Liaoning Petrochemical University, No.1 Dandong Road West Section, Wanghua District, Fushun 113001, Liaoning, China. E-mail: yangye56@163.com; lsong@lnpu.edu.cn

Abstract

Propane dehydrogenation (PDH) Pt-based catalysts are facing the serious challenge of coke deactivation. The locations would greatly influence the coke formation, while the detailed mechanism is not fully explored. Herein, the coke mechanisms on different locations including Al$_2$O$_3$, Sn, Pt, and Pt-Sn sites were deeply investigated via *in situ* Fourier transform infrared spectroscopy (FTIR) technology, and the key factors triggering catalyst coke deactivation were proposed. Excessive dehydrogenation of propyl species is a crucial initial step in the formation of coke, whether at metal sites or supports. These propyl species on Al$_2$O$_3$ supports then cyclize to form monocyclic aromatic and bicyclic aromatic species, while those on SnO$_x$ sites cyclize to form monocyclic aromatic species. As for the Al$_2$O$_3$ supported PtSn catalysts, the strong dehydrogenation function and the interaction between Pt and Al$_2$O$_3$ supports trigger the complex coke formation mechanism. The surface Pt sites with saturated coordination are prone to coke deposition, leading to rapid deactivation at the initial stage of the reaction. However, the low-coordination Pt sites with ultra-small size are found to be highly resistant to coke formation in the PDH reaction, which selectively catalytic the PDH. Owing to the metal-support interaction, the extensive active hydrogen species generated from Pt can regulate the formation of coke precursors on the Al$_2$O$_3$ supports. Furthermore, the effect of hydrogen co-feed on coke deposition is also explored. The hydrogen co-feed inhibits the coke formation and results

in a higher H/C ratio (3.96) for aromatic coke precursors. This study can enhance the understanding of the coke formation in PDH, which is important to designing efficient PDH Pt-based catalysts.

INTRODUCTION

Pt-based catalysts exhibit excellent catalytic activity in the direct dehydrogenation of propane to propylene, while they face a severe challenge of coke deactivation[1-4]. Frequent regeneration not only involves complex processes and huge energy consumption but also cannot fundamentally resolve the problem of coke deactivation[2,5]. Consequently, researchers have developed extensive optimized strategies from various perspectives to suppress coke deactivation, including constructing active phases, selecting carriers, enhancing interactions between metal and carriers, and controlling reaction pathways[6-10]. Among these, adding tin as a promoter to modify, both electronically and geometrically, the structure of the supported Pt on Al_2O_3 carriers is an effective approach[6,7]. Although this can alleviate the coke deposition problem to some extent, a large amount of coke still forms on the Al_2O_3 supported PtSn catalyst. A fundamental resolution to the coke deposition necessitates a deep understanding of the key initiation steps and the dynamic evolution mechanism of coke species in propane dehydrogenation (PDH).

The processes of coke formation are complicated, involving complex surface reactions and various intermediates in the PDH process[11,12]. The specific effect brought by coke accumulation significantly depends on the catalytic system and the location of coke deposition. In Pt-based catalysts, the coke positions have been studied, which are classified into three locations, i.e., metallic Pt, the boundary between the Pt and the support, and the support[13,14]. Researchers have associated different site characteristics with their propensity to cause coke deposition and discovered significant variations in the structure and properties of coke formed at different reaction sites[13].

Coke deposition initiated at metallic Pt active sites mainly originates from their strong dehydrogenation function. According to the current mechanism for the PDH reaction, propane molecules adsorb onto the metal sites and undergo two consecutive dehydrogenations, forming a propylene precursor that strongly adsorbs on the metal sites and undergoes excessive dehydrogenation, leading to the formation of coke[8,15]. Numerous studies indicate that larger Pt particles are prone to coke deposition, compared with the small-sized Pt clusters[16,17]. This is mainly attributed to the strong adsorption of propylene precursors on large-sized Pt particles, resulting in excessive dehydrogenation. Besides, the coordination structure of the Pt active phase can also affect coke formation. The coordination-saturated Pt active sites facilitate side reactions, such as C–C cleavage and deep dehydrogenation, thereby forming coke deposits[6,18].

The carrier is another crucial factor in the initiation of coke deposition[19]. Alumina, used as the carrier in industrial Pt-based PDH catalysts, has pronounced acidic characteristics that enable it to catalyze a series of side reactions, such as oligomerization, cyclization, and condensation of the desorbed product olefins, leading to the formation of coke with a high hydrogen-to-carbon ratio[20]. Numerous studies have shown that reducing the acidity of the carrier can significantly decrease the occurrence of cracking and polymerization reactions, enhance the selectivity for propylene in the modified samples, and markedly inhibit the coke deactivation of catalysts[21]. However, some investigators also proposed that when the acidity of the catalyst is too low, the coke amount increases rather than decreases[13,14]. They attributed it to the synergistic effect between metal and acidic sites that inhibited the formation of coke deposition. Therefore, it is evident that the formation of coke deposition during PDH is influenced by the carrier acidity

and the synergistic interaction between the carrier and metal sites.

In addition to metal sites and carriers, the reaction situation is a key factor affecting coke deposition behavior in PDH[8,12,22]. In practical propylene production, hydrogen as a co-feeding gas has been utilized to inhibit the deactivation rate, obviously improving the stability of Pt-based catalysts[23]. This inhibitory mechanism is usually attributed to two main factors: (i) the desorption barrier of propylene can be reduced; (ii) metallic active sites can be preserved with the existence of hydrogen[24]. However, the introduction of hydrogen has a large influence on the properties of metal sites and the support acidity, inevitably leading to different coke deposition behaviors.

Hydrogen dissociates at metal sites and forms metal-hydride species (M-H), which possess different adsorption capabilities for propylene precursors from the metallic active phase, thereby significantly influencing coke deposition[25-27]. The hydrogen spillover caused by the metallic Pt sites, forming active hydrogen species, also significantly impacts coke formation[28,29]. Besides, the spillover of these active hydrogen species onto the carrier can alter its surface properties[30,31], triggering another crucial factor of coke formation. Obviously, different sites and reaction situations substantially influence coke formation in PDH with a high degree of interconnectivity between them. Due to the complex interactions of the various factors and the complexity of the reaction mechanisms, the coke formation mechanisms at different sites in PDH are not yet well understood which evidently limits the progress in research on inhibiting coke deactivation. Revealing the coke formation mechanisms in the Pt-based catalyst system could significantly advance the development of de-coking technologies in the PDH field.

Herein, the Al_2O_3 supported PtSn catalyst, which is widely used and has excellent performance in PDH, is used as the research object. Starting with the key initiation steps of coke deposition in PDH, the formation mechanisms of coke at different locations are deeply analyzed using a Fourier transform infrared spectroscopy (FTIR) method, and an active site structure that does not undergo coke deactivation is proposed. More specifically, the relations between the location of coke, structures of active phase and coke deactivation mechanism are established. The FTIR spectra can provide very important information on the amount and nature of coke and on its effect on the catalyst acidity.

EXPERIMENTAL
Catalyst preparation
Al_2O_3 (99%, Sasol Germany GmbH) and $Sn-Al_2O_3$ (99%, Sasol Germany GmbH) were calcined at 650 °C for 4 h to make $\gamma-Al_2O_3$ support and $Sn-\gamma-Al_2O_3$, respectively. The obtained catalysts were named as the Al_2O_3 and $Sn-Al_2O_3$. The Sn content of the $Sn-Al_2O_3$ sample is 0.3 wt%.

The Pt/Al_2O_3 catalyst was synthesized by a wet impregnation method, in which the theoretical amount of Pt was 0.5 wt%. First, 13.25 mg of $H_2PtCl_6 \cdot 6H_2O$ (99.5%, Sinopharm Chemical Reagent Co. Ltd.) were diluted in appropriate amounts of water. Subsequently, the solution containing the metal precursors was impregnated into 1.0 g of the above calcined Al_2O_3. After impregnation, the samples were stirred for 15 min, maintained at room temperature for 6 h, and then dried at 50 °C for 12 h. This was followed by calcination in 20% O_2/N_2 at 600 °C for 2 h. Sample reduction was conducted in pure H_2 atmosphere at 500 °C for 1 h. The obtained catalysts were named as the Pt/Al_2O_3. As for the $Pt/Sn-Al_2O_3$, the calcined $Sn-Al_2O_3$ was chosen as a carrier on which to load the $H_2PtCl_6 \cdot 6H_2O$ using the same preparation procedure. The obtained catalysts were named as the $Pt/Sn-Al_2O_3$.

Catalyst characterization

The crystalline structures of the samples were confirmed using a Bruker D8 Advance X-ray diffraction (XRD) instrument. This analysis was conducted using Cu Kα radiation, characterized by a wavelength of 0.154 nm, under an operating voltage of 3 kV. A transmission electron microscopy (TEM) image was recorded on a JEOL-2100F microscope, which was operated at an accelerating voltage of 200 kV. The analysis utilizing X-ray photoelectron spectroscopy (XPS) was conducted employing an ESCALAB Xi+ instrument from Thermo Fisher Scientific, which utilized Al Kα radiation for the X-ray source. All samples underwent a reduction process at 500 °C for 1 h in an atmosphere of pure H_2, after which they were hermetically sealed and stored in vials. The hydrogen temperature programmed reduction (H_2-TPR) analysis was executed using a BSD-Chem C200 system. This involved flowing a 10% H_2/Ar mixture (with a flow rate of 30 mL/min) over a 100 mg sample (with a particle size of 40-60 mesh), while heating at a rate of 10 °C/min per minute until reaching 700 °C. The hydrogen temperature programmed desorption (H_2-TPD) analysis was conducted using a BSD-Chem C200 device. In a typical procedure, 50 mg of the catalyst was initially treated under a 10% H_2/Ar flow (30 mL/min) at 500 °C for 2 h, followed by a 30-minute He purge at the same flow rate. To facilitate hydrogen absorption, a H_2/Ar mixture was flowed over the catalyst for 30 min at 30 mL/min, followed by a He purge for 1 h. Subsequently, the sample was heated to 700 °C at 5 °C/min under He flows (30 mL/min). The ammonia temperature programmed desorption (NH_3-TPD) followed the same experimental procedure. The amount of coke deposited was determined using a STA 449 F3 thermogravimetric (TG) analyzer from NETZSCH. The catalyst, weighing 15 mg, underwent He flow (40 mL/min) at 200 °C for 1 h, followed by a cooldown to room temperature. Subsequently, the catalyst was heated from room temperature to 950 °C at a rate of 5 °C/min under 20% O_2/N_2 (40 mL/min). Raman spectroscopy was performed to investigate the coke properties on a Thermo Fisher DXR Raman spectrometer with a 532 nm laser beam. The laser power, resolution of the apparatus and data acquisition time were 0.1 mW, 2 cm^{-1} and 10 s, respectively. An inverted configuration of the Nikon AX was used for the confocal fluorescence microscopy studies. All crystals have been measured using a 100 1.0 AU oil objective lens. The fluorescence images were collected using a Nikon AX scan head connected to laser light sources 405, 488, 561 and 640 nm, while the detection area is full spectrum detection with a photomultiplier tube (PMT).

FTIR spectra were recorded on a Thermo Scientific Nicolet iS50 FTIR spectrometer. All spectra were collected as an average of 64 scans at 4 cm^{-1} resolutions. The difference spectrum is obtained by subtracting the collected infrared (IR) spectra from the background spectra. (1) CO-adsorption experiment: the sample was initially reduced with H_2/Ar (30 mL/min) for 1 h and subsequently cooled to 30 °C. Following this, it was exposed to a 10% CO/Ar mixture until equilibrium was reached. Then, the cell was purged with Ar flow to remove the physically adsorbed CO, with IR spectra being gathered continuously until stabilization; (2) Pyridine-adsorption experiment: the samples were activated at 400 °C for 2 h under a vacuum setup (< 10^{-3} Pa). The sample was subjected to pyridine vapor at 150 °C for 30 min. FTIR spectra were then recorded after degassing at 150 and 400 °C for 1 h; (3) C_3H_8-dosing and C_3H_8/H_2-dosing experiment: the sample was reduced at 500 °C for 1 h under 10% H_2/Ar (30 mL/min). In Ar atmosphere, the temperature was raised to 600 °C to collect the background spectrum. The pulse experiments were carried out at 600 °C by pulses of pure propane or C_3H_8/H_2 mixture (volume ratio = 1:1) [pulse volume = 0.50 cm^3 standard temperature and pressure (STP)] to the *in situ* cell, which was maintained under Ar flow (30 mL/min). After the pulse, FTIR spectra were continuously recorded for five minutes; (4) The isotope exchange reactions with hydrogen and deuterium (H/D) and C_3H_8-dosing experiment: the sample was evacuated (< 10^{-3} Pa) at 400 °C for 1 h, and the background spectrum was collected. Then, the sample was exposed to D_2O vapor until adsorption saturation. The completely deuterated sample was fed 500 Pa of propane at 400 °C; (5) C_3H_8 Multiple pulse experiments: the propane pulse experiment procedure is the same as in Part (3). After pulsing propane at 600 °C, the sample was cooled to 30 °C for CO adsorption, using the procedure in Part

(1). Following complete CO desorption, the temperature was raised back to 600 °C for a new round of propane pulsing. The IR spectra after 1-10 rounds of propane pulsing and *in-situ* FTIR spectra of CO adsorption after rounds 1-2 and 9-10 were recorded.

Catalytic tests

The PDH performance was conducted in a tubular quartz reactor with a fixed bed under atmospheric pressure. The reactor's temperature was regulated using a Golden Eagle temperature controller (Series 708P). In each test, 0.1 g of the catalyst was utilized. A gaseous mixture containing C_3H_8 and H_2 in a 1:1 volume ratio was introduced over the catalyst layer at 600 °C. Product analysis was performed using an inline gas chromatograph. For the separation and detection of H_2, C_3H_8, C_3H_6, C_2H_4, C_2H_6, CH_4, and C_4-C_6 in the effluent, KB-1 (8 m × 0.32 mm × 0.50 μm) and TDX-01 (3 mm × 1 m) columns were employed. The conversion of propane and the selectivity for the various products were determined by:

Propane conversion:

$$\text{Conv. (\%)} = ([C_3H_8]_{in} - [C_3H_8]_{out})/[C_3H_8]_{in} \times 100 \tag{1}$$

Selectivity of products:

$$\text{Selectivity (\%)} = [C_3H_6]_{out}/([C_3H_8]_{in} - [C_3H_8]_{out}) \times 100 \tag{2}$$

where $[C_3H_8]_{in}$, $[C_3H_8]_{out}$ and $[C_3H_6]_{out}$ were the imported molar concentration of C_3H_8, the outlet molar concentration of C_3H_8 and C_3H_6 in the effluent gas, respectively.

RESULTS AND DISCUSSION

Evolution path of coke precursors on different sites of Al_2O_3 supported PtSn catalysts

The coke formation on Al_2O_3 supported PtSn catalysts primarily occurs at metal sites, metal-support interface and supports, with distinct mechanisms at each location. However, the current research on the coke deposition mechanism at different sites and the interactive effects between various sites remain unclear [Supplementary Table 1]. To investigate the coke formation mechanisms at these sites, four model catalysts, Al_2O_3, Sn/Al_2O_3, Pt/Al_2O_3, and $Pt/Sn-Al_2O_3$, were designed and prepared. All samples maintain the typical crystal phase structure of γ-Al_2O_3 [Supplementary Figure 1] but have different active components. These four catalysts exhibit similar crystalline morphology and size [Supplementary Figures 2 and 3].

To investigate the formation mechanism of coke precursors on catalysts, a hyphenated technique combining pulse, high temperature and *in situ* IR spectroscopy was utilized to analyze the types and formation mechanisms of these precursors [Figure 1]. The pulse experiments were carried out at 600 °C by pulses of pure propane (pulse volume = 0.50 cm³ STP) to the *in-situ* cell, which was maintained under Ar flow (30 mL/min). After the pulse, FTIR spectra were continuously recorded for five minutes. Table 1 exhibits the summary of the vibrational modes and positions of adsorption peaks. When 0.5 mL of C_3H_8 is pulsed into the *in situ* cell at 600 °C, strong absorption peaks at 2,872-2,985 cm⁻¹ attributed to the stretching vibrations of methyl C–H bonds in C_3H_8 are observed [Figure 1][32,33]. These four catalysts show distinct formation processes of coke precursor due to differences in their active components.

For the Al_2O_3 sample, four peaks between 1,372 and 1,450 cm⁻¹ attributed to the bending vibrations of C–H in CH_2 and CH_3 groups are observed at the initial stage of pulsing propane [Figure 1A]. Specifically, the peak at 1,450 cm⁻¹ is associated with 1-propyl and 2-propyl vibrations, 1,396 cm⁻¹ with 1-propylidene and
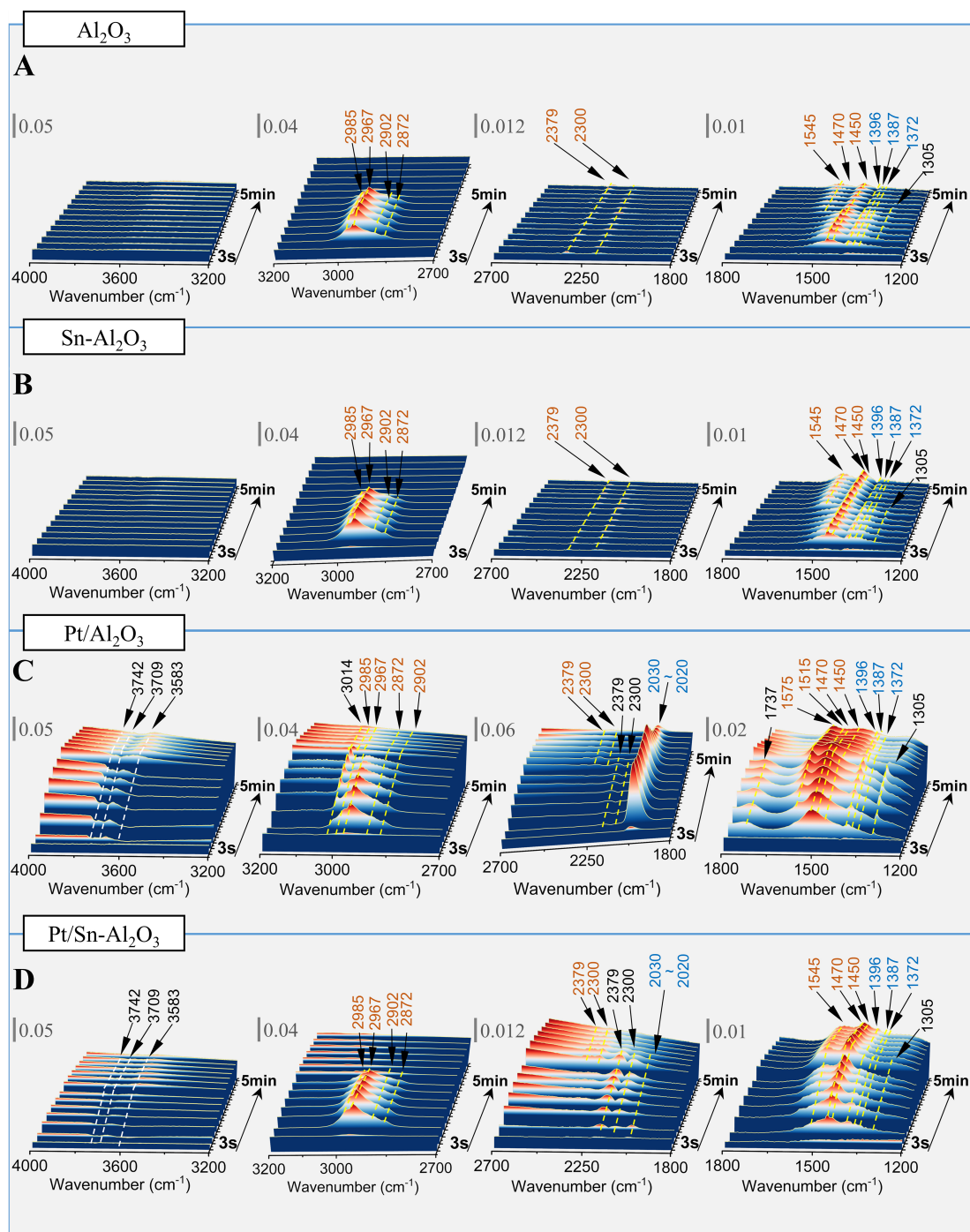
Figure 1. The coke mechanism of PDH on various locations. FTIR differential spectra following propane pulse adsorption for (A) Al_2O_3, (B) $Sn\text{-}Al_2O_3$, (C) Pt/Al_2O_3 and (D) $Pt/Sn\text{-}Al_2O_3$. The pulse experiments were carried out at 600 °C by pulses of pure propane (pulse volume = 0.50 cm^3 STP) to the *in situ* cell at Ar (30 mL/min) atmosphere. The yellow dashed line represents the adsorption peak, while the white dashed line represents the inverted peak caused by the occupation of adsorption sites. PDH: Propane dehydrogenation; FTIR: Fourier transform infrared spectroscopy; STP: standard temperature and pressure.

2-propylidene, 1,372 and 1,387 cm^{-1} with 1-propylidyne, and 1,305 cm^{-1} with olefinic C–H stretching vibration[34,35]. These vibrational peaks persist after Ar purging, indicating chemical rather than physical adsorption. It can be seen that propane undergoes dehydrogenation on the Al_2O_3 surface. According to

**Table 1. Summary of the vibrational modes and positions of adsorption peaks (1,200-4,000 cm^{-1})**

Species	Vibrational mode	Band position (cm^{-1})	
		This work	Literature range
Olefin	δ_m (C–H)	1,305	1,295-1,310[34]
1-Propylidyne	δ_s (C–H)	1,372, 1,387	1,370-1,377[34,35]
1-Propylidene 2-Propylidene	δ_s (C–H)	1,396	1,392-1,398[34,35]
1-Propyl 2-Propyl	δ_s (C–H)	1,450	1,450-1,458[34,35]
Benzene	ν (C=C)	1,470	1,450-1,650[43-46]
Naphthalene	ν (C=C)	1,545	1,488-1,545[43-46]
Polyaromatic	ν (C=C)	1,575	1,575-1,602[43-46]
Acetone	δ_s (C–H) ν (C=O) δ (C–H)	3,014 1,737 1,440	3,000-3,300[40] 1,668-1,725[40-42] 1,434-1,436[40-42]
Alkyne	ν (C≡C)	2,104-2,190	2,100-2,260[43]
Propane Al$_2$O$_3$	ν_{vs} (C=C) ν_{vs} (H–O)	2,985-2,872 3,700-3,200	2,875-2,990[44] 3,200-3,700[45]

NH$_3$-TPD and Py-FTIR results [Supplementary Figures 4 and 5], the Al$_2$O$_3$ possesses numerous medium-strong acid sites[36], predominantly as Lewis acid sites at tri-coordinated Al defect sites [Supplementary Figure 6][37-41]. Therefore, it is believed that propane molecules undergo successive dehydrogenation reactions at these Lewis acid sites of Al$_2$O$_3$. Wang *et al.* also proposed that this type of tri-coordinated Al defect site with Lewis acidity can catalyze the dehydrogenation of propane[42]. The C–H bonds in propane are activated at Al$_{III}$ sites, forming an Al$_{IV}$-C$_3$H$_7$ species. Initially, the C–H bonds in propane are broken by proton abstraction by surface oxygen atoms, leading to bonding of propyl with surface aluminum to form the Al$_{IV}$-C$_3$H$_7$ surface species. In the second step, β-hydrogen is eliminated from Al$_{IV}$-C$_3$H$_7$, yielding H$_2$ and propylene products, as illustrated in Scheme 1. Therefore, these 1-propylidene, 2-propylidene and 1-propylidyne formed on Al$_2$O$_3$ are the main precursor triggering coke species. A comparison of the product distribution in PDH for Al$_2$O$_3$ samples reveals that the primary gaseous products are propylene, ethylene, and methane resulting from cracking [Supplementary Figure 7]. With increasing reaction time, the content of ethylene remains higher than that of methane and does not show a significant decline, suggesting that ethylene formed from cracking does not undergo further reactions and is not the key species triggering coke formation. Instead, the formation of coke precursors is due to the deep dehydrogenation of propyl species at strong Lewis acid sites [Scheme 1].

Furthermore, the FTIR spectrum of Al$_2$O$_3$ also exhibits absorption peaks at 1,470-1,600 cm^{-1} and 2,100-2,400 cm^{-1} [Figure 1A]. The peaks at 1,470 and 1,545 cm^{-1} are attributed to the C=C stretching vibrations of monocyclic and bicyclic aromatic species, respectively[43-48]. The peaks at 2,190 and 2,300-2,380 cm^{-1} correspond to the C≡C stretching vibration of alkynes and C=C=C stretching vibrations of dienes. With the increase of reaction time, the peak at 1,470 cm^{-1} increases first and then shows a declining trend, while the peak at 1,545 cm^{-1} gradually forms and grows. These results indicate that the coke formation pathway on the Al$_2$O$_3$ surface starts with deep dehydrogenation of propene to form propylidene and 1-propylidyne species, which then gradually cyclizes to form substituted monocyclic aromatic species. As the reaction intensifies, these monocyclic aromatic species further dehydrogenate and cyclize to form polyaromatic species [Scheme 2].
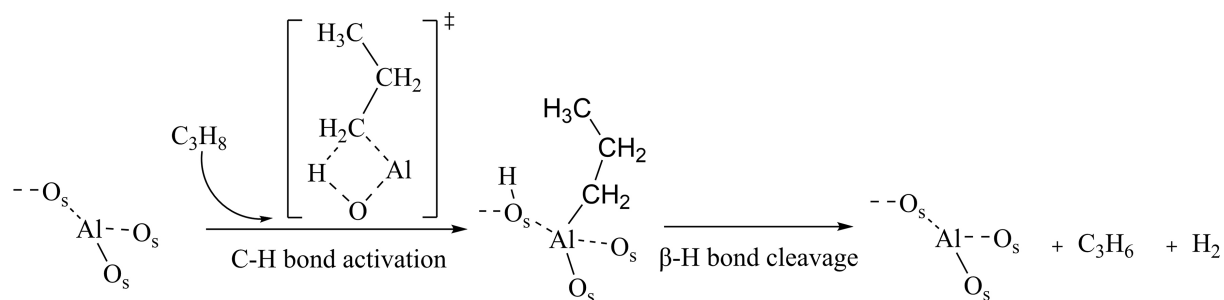
Scheme 1. Reaction mechanism for PDH on the Al_2O_3 sample. PDH: Propane dehydrogenation.
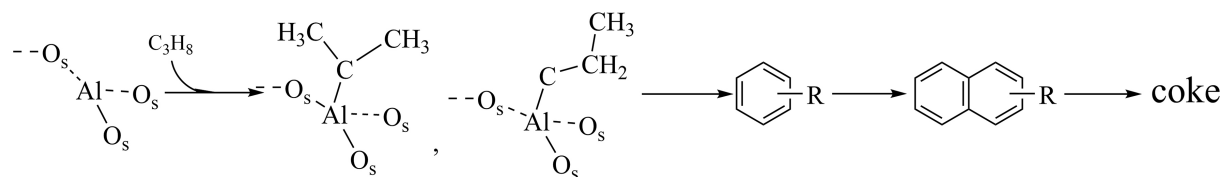
Scheme 2. Formation mechanism of coke precursors on the Al_2O_3 sample.

Doping Sn species into alumina alters its acidity. Similar to alumina, Sn-Al_2O_3 only contains Lewis acid sites, but both its acid amount and strength are significantly higher than those of Al_2O_3 [Supplementary Figures 4 and 5][49]. XPS results show that the Sn species in Sn-Al_2O_3 mainly exists in the form of Sn^{4+} [Supplementary Figure 8]. This is further confirmed by the absence of significant Sn species reduction peaks in H_2-TPR of Sn-Al_2O_3 [Supplementary Figure 9][50]. These results indicate that the main Sn species in Sn-Al_2O_3 is SnO_x. Therefore, the acidity change in the Sn-Al_2O_3 catalyst primarily originates from SnO_x species, which show Lewis acidity. When pulsing propane into the Sn-Al_2O_3 catalyst, the absorption peaks at 1,396, 1,470, and 1,545 cm^{-1} intensify [Figure 1B]. The intensities of peaks at 1,470 and 1,545 cm^{-1} belonging to C=C stretching vibrations for monocyclic and polycyclic aromatic species in Sn-Al_2O_3 are notably higher than those in Al_2O_3, indicating that the stronger acid strength and higher acid amount of the Sn-Al_2O_3 sample lead to the formation of more coke. Notably, the peak strength of monocyclic aromatic does not decrease with the formation of polycyclic aromatics, suggesting that a large amount of monocyclic aromatics forms without further transforming into polycyclic aromatics. Combining the coke formation mechanism on Al_2O_3 [Scheme 2], polycyclic coke formation primarily originates from coke deposition on the Al_2O_3 support, while SnO_x sites predominantly produce monocyclic aromatic coke precursors. Wang *et al.* also found that the introduction of SnO_x species could facilitate the decarbonylation of acetone to form xylene in Sn-HZSM-5 catalysts[51]. Hence, SnO_x sites mainly catalyze the deep dehydrogenation of propane to form monocyclic aromatic coke precursor species [Scheme 3].

After loading Pt, its strong dehydrogenation capability significantly influences the coke deposition mechanism on the catalyst, warranting a discussion on the formation mechanism of coke precursors on Pt/Al_2O_3 [Figure 1C]. Compared to Al_2O_3 and Sn-Al_2O_3 catalysts [Figure 1A and B], the intensity of δ_s (C–H) absorption peaks for propylidene and propyl groups at 1,372-1,450 cm^{-1}, and δ_m (C–H) absorption peaks for olefins at 1,305 cm^{-1} significantly increase. This indicates intense dehydrogenation reactions of C_3H_8 molecules at Pt sites with strong dehydrogenation ability, forming a large amount of propyl and olefin species. The intensity of peak at 2,104-2,190 cm^{-1} increases with the intensification of the peaks at 1,305-1,396 cm^{-1}. Hence, further dehydrogenation of propylidyne can form adsorbed diene or acetylene species, whose further cyclization can produce monocyclic aromatics. Different from the Al_2O_3 and Sn-Al_2O_3 catalysts [Figure 1A and B], the Pt/Al_2O_3 catalyst rapidly forms a strong vibration peak at 1,515 cm^{-1} at the
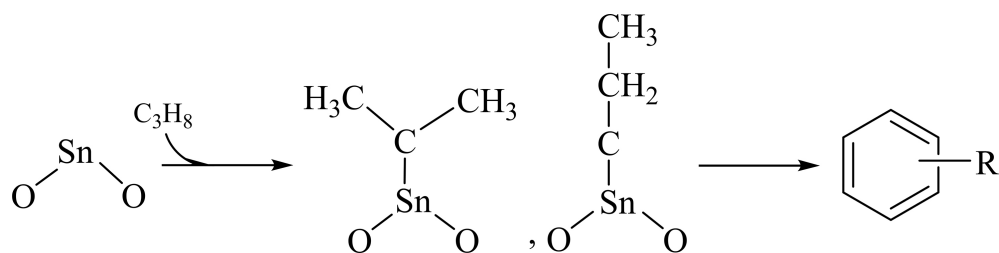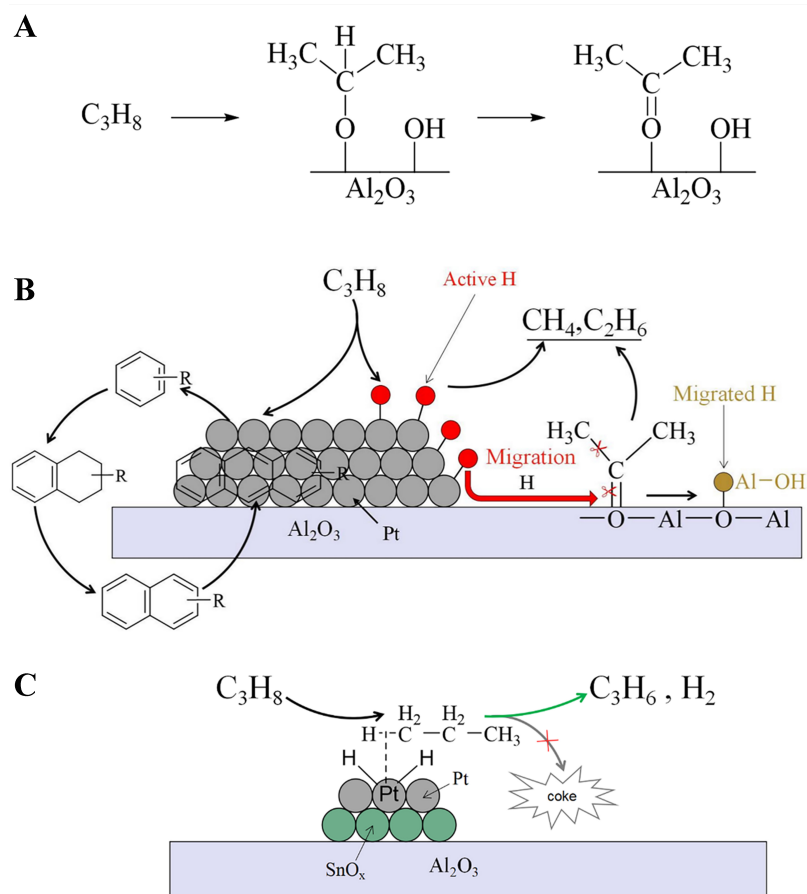
Scheme 3. Formation mechanism of coke precursors on the Sn-Al$_2$O$_3$ sample.

reaction onset, situated between the peak of polycyclic aromatics at 1,545 cm^{-1} and the peak of monocyclic aromatics at 1,470 cm^{-1}. This peak is attributed to the cycloalkyl benzene coke precursors[52,53]. As the peak areas of monocyclic aromatics at 1,470 cm^{-1} and cycloalkyl benzene species at 1,515 cm^{-1} decrease, the polycyclic aromatic peak at 1,575 increases, suggesting that the polycyclic aromatic coke precursors are primarily derived from the condensation of monocyclic aromatic and cycloalkyl benzene species.

Interestingly, an absorption peak at ~1,737 cm^{-1} is observed in the Pt/Al$_2$O$_3$ [Figure 1C], which is attributed to the ν (C–O) vibration[54,55]. Concurrently, a significant negative peak appears at 3,600-3,800 cm^{-1}, indicating that the hydroxyl groups in the alumina are occupied. These results suggest that the C in coke precursors is linked to O in Al$_2$O$_3$, forming C–O bonds. Airaksinen *et al.* and Finocchio *et al.* also reported the presence of acetone-like species in coke precursors on alumina, which further confirms the formation of the C–O bonds in our study[56,57]. Comparative analysis of the change in these C–O species absorption peaks during the reaction indicates that the concentration of C–O species initially increases rapidly with reaction time, then gradually decreases until it completely vanishes. Notably, the absorption peak of C–O species was only observed in the FTIR difference spectra of Pt/Al$_2$O$_3$ sample, not in Al$_2$O$_3$ or Sn-Al$_2$O$_3$ [Figure 1A and B], suggesting a close correlation between the formation of C–O species and Pt active sites in Pt/Al$_2$O$_3$ [Scheme 4A]. Given the strong dehydrogenation capability of Pt active sites, the dynamic changes of C–O species are highly correlated with Pt sites.

Another significant difference between Pt/Al$_2$O$_3$ [Figure 1C] and Al$_2$O$_3$ [Figure 1A] or Sn-Al$_2$O$_3$ [Figure 1B] is the strong absorption peak at 2,020-2,030 cm^{-1}, which is attributed to Pt–H species or active hydrogen species produced by the activation of hydrogen on Pt sites[58]. The large amount of hydrogen spillover desorption peaks at 200-500 °C in H$_2$-TPD for Pt/Al$_2$O$_3$ further confirms substantial active hydrogen species [Supplementary Figure 10]. There is a correlation between active hydrogen species and C–O species absorption peaks. The formation of active hydrogen species is accompanied by the appearance of C–O species. As the C–O species decrease, the content of active hydrogen species also diminishes, and the corresponding inverted peak at the surface hydroxyl groups becomes significantly smaller. This indicates that active hydrogen spills over from Pt sites to the support surface, reacting with C–O species to form hydrocarbon molecules, thereby restoring the alumina hydroxyl groups [Scheme 4B].

Based on scanning transmission electron microscopy (STEM) [Supplementary Figure 3] and CO adsorption IR spectroscopy [Supplementary Figure 11] results, the geometric effect of Sn leads to a smaller size of metal clusters in the Pt/Sn-Al$_2$O$_3$ catalyst (1.51 nm) compared to Pt/Al$_2$O$_3$ (1.74 nm). XPS and H$_2$-TPR results confirm that Pt species in the Pt/Sn-Al$_2$O$_3$ catalyst exist in a lower coordination number and a partially oxidized state [Supplementary Figures 9 and 12, Supplementary Table 2][59-61]. Correspondingly, the main Sn species in the Pt/Sn-Al$_2$O$_3$ catalyst consist of Sn^{4+} (495.5, 487.0 eV) accounting for 74.0%, Sn^{2+} (494.6, 486.2 eV) for 4.4%, and Sn^0 (492.7, 484.4 eV) for 21.5% [Supplementary Figure 8, Supplementary Table 3]. In this case, the interface structure between Pt and Sn species primarily comprises the structure of Pt-SnO$_x$-

A

B

C

Scheme 4. (A) The deep dehydrogenation of propane at the oxygen species of Al_2O_3 support in Pt/Al_2O_3 sample; (B) Formation mechanism of the coke precursor and dehydrogenation mechanism on Pt/Al_2O_3 in PDH, the red ball and line represent the active hydrogen species; (C) Formation mechanism of the coke precursor and dehydrogenation mechanism on the $Pt/Sn-Al_2O_3$ catalyst. PDH: Propane dehydrogenation.

Al_2O_3, which agrees with the previous results[62-65]. The introduction of Sn effectively regulates the geometric and electronic structures of Pt[66], affecting the formation of coke precursors. As shown in the FTIR spectrum of the $Pt/Sn-Al_2O_3$ catalyst [Figure 1D], the vibration peak of olefins at 1,470-1,600 cm^{-1} is observed, along with absorption peaks for monocyclic and polyaromatic species. There is a dynamic transition from monocyclic to bicyclic naphthalene species. Interestingly, the $Pt/Sn-Al_2O_3$ catalyst does not exhibit the absorption peak at 1,575 cm^{-1}, and the overall intensity of its IR absorption peaks is weaker than that of Pt/Al_2O_3. This suggests that the reactivity of $Pt/Sn-Al_2O_3$ is milder, focusing primarily on monocyclic and bicyclic aromatic species rather than the more heavily cyclized polycyclic aromatic hydrocarbons.

The 2,020-2,031 cm^{-1} region is attributed to the vibrational peaks resulting from the interaction between hydrogen and Pt. Compared to the Pt/Al_2O_3 catalyst [Figure 1C], the peak of Pt–H species in the $Pt/Sn-Al_2O_3$ catalyst is mainly concentrated at a lower wavenumber ~2,020 cm^{-1}, with a lower peak intensity [Figure 1D]. Combined with H_2-TPD results [Supplementary Figure 10], the desorption peak area of hydrogen spillover of the $Pt/Sn-Al_2O_3$ catalyst is significantly lower than that of the Pt/Al_2O_3 catalyst. This indicates that the reduction in active hydrogen content due to hydrogen spillover leads to a decrease in peak intensity at the 2,020-2,031 cm^{-1}. In H_2-TPD [Supplementary Figure 10], hydrogen spillover occurs at higher temperatures, which are energy-intensive. According to FTIR analysis of vibrational characteristics, the

peak at 2,031 cm^{-1} is assigned to active hydrogen species, while the peak at 2,020 cm^{-1} is attributed to Pt–H species [Figure 1C and D]. The Pt–H species are an efficient active site for PDH. Correspondingly, there is a slight recovery in the hydroxyl region (3,200-4,000 cm^{-1}) after a reduction in hydroxyl coverage, but this recovery is much less significant than in Pt/Al$_2$O$_3$. This further indicates that SnO$_x$ species in the Pt/Sn-Al$_2$O$_3$ catalyst regulate Pt to suppress the formation of active hydrogen. Compared to other catalysts, SnO$_x$ species promote the formation of Pt–H bonds, establishing efficient active sites for PDH to propylene [Scheme 4C].

Key factors affecting coke deposition of Al$_2$O$_3$ supported PtSn catalysts

Structures of Pt active phase

The coke formation mechanism on Pt active sites is proposed, but various Pt active sites are observed in *in-situ* FTIR spectra of CO adsorption which can affect the formation of coke precursors. For instance, the linear adsorption peaks at 2,060 and 2,040 cm^{-1} correspond to high-coordination and low-coordination Pt species, respectively, and the bridge adsorption peak at 1,800 cm^{-1} [Supplementary Figure 11]. To investigate the influence of different Pt active phase structures on coke deposition, we designed multiple pulse experiments to observe the correlation between coke precursor generation and the structure of Pt active sites. After pulsing propane at 600 °C, the Pt/Sn-Al$_2$O$_3$ catalyst was cooled to 30 °C for CO adsorption analysis. Following complete CO desorption, the temperature was raised back to 600 °C for a new round of propane pulsing. The IR spectra after 1-10 rounds of propane pulsing [Figure 2] and *in-situ* FTIR spectra of CO adsorption after rounds 1-2 and 9-10 [Figure 3] were recorded.

Figure 2D shows that with increasing pulse numbers, the intensity of the absorption peaks at 1,470 and 1,545 cm^{-1} gradually rises, indicating the formation of monocyclic and polyaromatic hydrocarbon species. At the same time, the stretching vibrations of aromatic substituents or unsaturated hydrocarbons at 2,300-2,380 cm^{-1} (C=C=C) and the stretching vibration of unsaturated hydrocarbons at 2,190 cm^{-1} (C≡C) slightly increase [Figure 2C], attributed to aromatic substituents and unsaturated hydrocarbon species formed by deep dehydrogenation. This indicates that with the increasing number of pulses, monocyclic and polycyclic aromatic hydrocarbon precursors with alkyl substituents continuously form and deposit on the Pt sites. As the formation of coke precursor species, the gradual decrease in intensity within the 3,767-3,784 cm^{-1} hydroxyl region suggests that the surface hydroxyl groups of supports are covered by coke precursors [Figure 2A]. Combining the above analysis, a positive correlation is observed between the number of propane pulsing cycles and the content of aromatic species. The reduction in hydroxyl content suggests that coke deposition occurs not only at Pt sites but also on the surface of the Al$_2$O$_3$ support.

The intriguing observation from Figure 2D is that the rate of coke deposition during the first 1-2 pulsing cycles is significantly higher than during the 9-10 cycles. This demonstrates a shift in the coke deposition sites. Therefore, we attempt to elucidate the relationship between coke precursors and various Pt sites using *in-situ* FTIR spectra of CO adsorption [Figure 3]; the intensity of CO adsorption peaks on Pt active sites decreases as the number of pulsing cycles grows. This suggests that coke precursors poison parts of Pt sites. The linear CO adsorption peak for fresh catalysts is predominantly at 2,060 cm^{-1}, shifting mainly to 2,040 cm^{-1} after the first pulsing cycle, with the emergence of an adsorption peak at 1,925 cm^{-1} attributed to CO adsorption on ultra-small Pt clusters[61]. This indicates that surface Pt sites with saturated coordination are firstly poisoned, while smaller-size and low-coordinated Pt sites (edge and corner sites of metal clusters) are not covered by coke deposition. After several pulsing cycles, the CO adsorption peaks are primarily at 2,040 and 1,925 cm^{-1}. It is worth noting that the peak at 2,060 cm^{-1} completely disappeared, while the peaks at 2,040 and 1,925 cm^{-1} contain no significant changes after the 9-10th pulsing cycles. In this case, the Pt sites in catalyst mainly consist of small-size and low-coordination Pt active phase, which is unaffected by coke precursors.
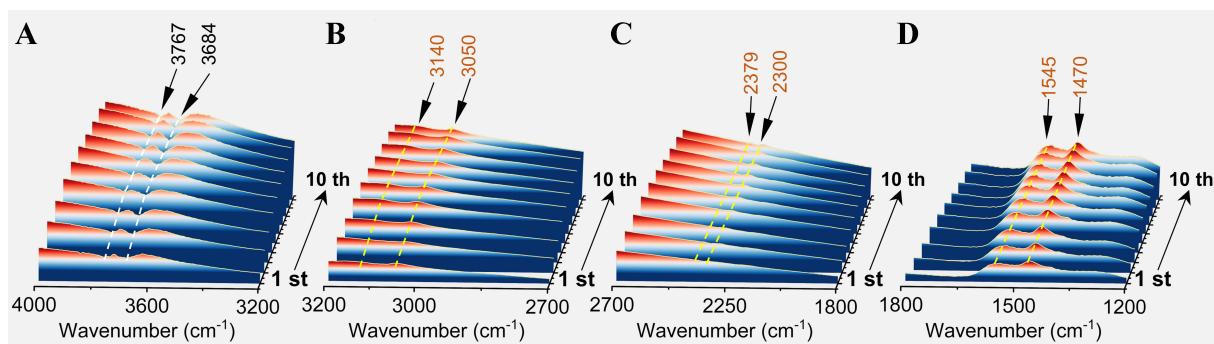
Figure 2. FTIR differential spectra of Pt/Sn-Al$_2$O$_3$ at 600 °C with different numbers of pulses of propane. (A) 4,000-3,200 cm^{-1}; (B) 3,200-2,700 cm^{-1}; (C) 2,700-1,800 cm^{-1}; (D) 1,800-1,200 cm^{-1}. The pulse experiments were carried out at 600 °C by pulses of pure propane (pulse volume = 0.50 cm^3 STP) to the *in situ* cell, which was maintained under Ar flow (30 mL/min) between two successive pulses. The yellow dashed line represents the adsorption peak, while the white dashed line represents the inverted peak caused by the occupation of the adsorption site. FTIR: Fourier transform infrared spectroscopy; STP: standard temperature and pressure.
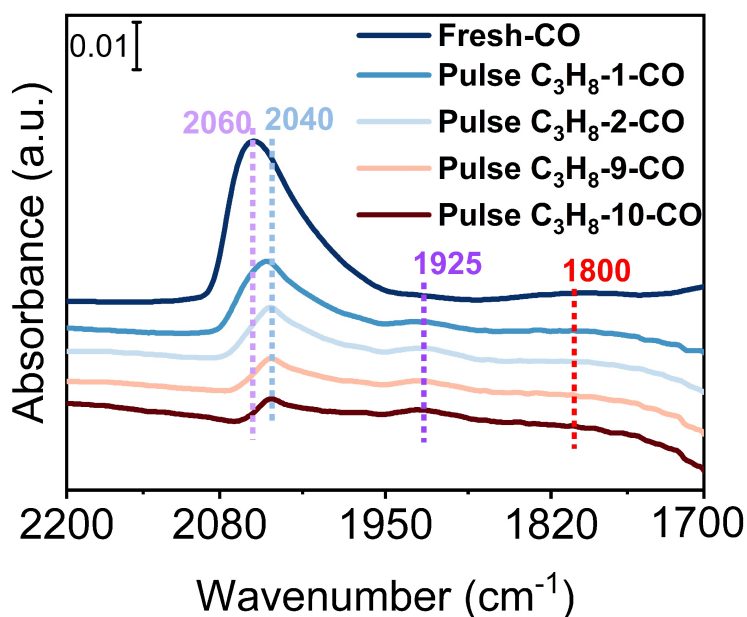

Figure 3. FTIR differential spectra of CO adsorption on the Pt/Sn-Al$_2$O$_3$ sample after pulse propane and reaction completion. After each pulse experiment, the sample was cooled to 30 °C, and the spectrum was collected after adsorption and desorption of CO. The temperature was raised to 600 °C for the next propane pulse experiment. The CO adsorption FTIR spectra of periods 1-2 and 9-10 were collected. FTIR: Fourier transform infrared spectroscopy.

This can also be confirmed by the correlation between PDH performance and coke deposition behavior of different Pt clusters [Figure 4]. The initial conversion of propane over the Pt/Al$_2$O$_3$ catalyst is 74.5%, which rapidly decreases to 49.2% after 1 h of reaction, a decline of 25.3% [Figure 4A]. This rapid decrease in activity is due to the extensive coke formed on surface Pt sites with saturated coordination [Figure 3, Supplementary Figure 11]. As coke extensively forms and covers these surface Pt sites with saturated coordination, the decreased rate of propane conversion slows down significantly after 1 h, indicating that the left Pt active sites have a strong capability to inhibit coke formation. These Pt active sites exist as low-coordination Pt sites with ultra-small size [Figure 3, Supplementary Figure 11]. As for the Pt/Sn-Al$_2$O$_3$ catalyst, the Sn can regulate Pt species to form more low-coordination Pt sites with ultra-small size, resulting in a slower deactivation of the Pt/Sn-Al$_2$O$_3$ catalyst. The initial conversion decreases from 33.2% to
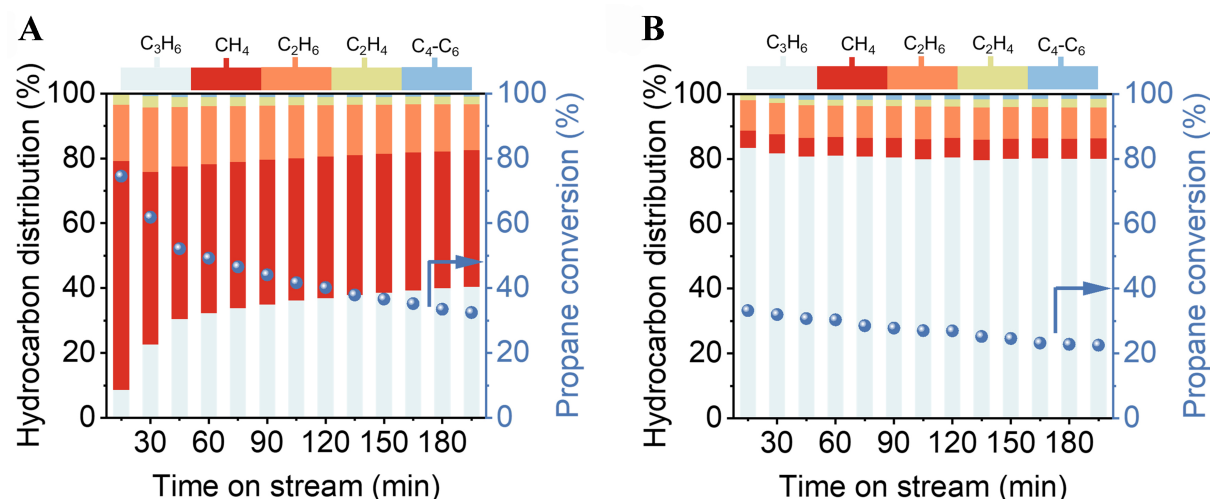
Figure 4. Product distribution of different catalysts as a function of time on stream during PDH for (A) Pt/Al$_2$O$_3$ and (B) Pt/Sn-Al$_2$O$_3$ samples. Dehydrogenation conditions: m$_{catalyst}$ = 100 mg, C$_3$H$_8$/H$_2$ = 1/1 (2.3 mL/min of propane and 2.3 mL/min of H$_2$), T$_{reduction}$ = 500 °C, T$_{reaction}$ = 600 °C, GHSV = 1,000. PDH: Propane dehydrogenation; GHSV: gas hourly space velocity.

22.5%, a reduction of only 10.7% [Figure 4B]. However, due to the electronic regulation of Pt by Sn, the conversion of Pt/Sn-Al$_2$O$_3$ catalyst is also reduced, which is significantly lower than the thermodynamic equilibrium conversion (~52%) under the same reaction condition [Supplementary Figure 7]. To further investigate the stability of the catalyst, a 100 h of PDH reaction was conducted for the Pt/Sn-Al$_2$O$_3$ catalyst [Supplementary Figure 13]. The propane conversion of Pt/Sn-Al$_2$O$_3$ gradually decreases as the reaction progresses, stabilizing at ~8% after approximately 50 h. Integrating these findings, the continued increase in coke deposition precursors and the sustained decrease in hydroxyl content, despite Pt sites no longer being affected, indicate that the carrier surface is the primary site of coke deposition.

Al$_2$O$_3$ carriers
Figure 5 shows the TG and corresponding differential TG (DTG) curves of catalysts after 3 h of PDH reaction. The degrees of weight loss in various catalysts increase in the order of Al$_2$O$_3$ (1.4%) < Sn-Al$_2$O$_3$ (1.9%) < Pt/Sn-Al$_2$O$_3$ (5.4%) < Pt/Al$_2$O$_3$ (18.5%) [Figure 5A]. The first weight loss peak within the 300-450 °C is attributed to coke at metal sites, while the peak within the 450-600 °C corresponds to coke on Al$_2$O$_3$ supports [Figure 5B]. Despite the lower coke content on the Al$_2$O$_3$, a peak in the high-temperature region suggests the formation of coke on the Al$_2$O$_3$ support. For the Sn-Al$_2$O$_3$ catalyst, weight loss is observed in both high- and low-temperature regions, with the high-temperature peak mainly due to coke on the support surface, and the low-temperature peak associated with monocyclic aromatic coke on SnO$_x$ species, as indicated by above FTIR analysis [Figure 1B]. The peaks for the Pt/Al$_2$O$_3$ catalyst are predominantly in the low-temperature region, suggesting that extensive coke deposition occurs on the Pt metal sites. The Pt/Sn-Al$_2$O$_3$ sample shows significant weight loss not only in the 300-400 °C range but also between 500-600 °C, confirming substantial coke accumulation on the Pt/Sn-Al$_2$O$_3$ support. Notably, the coke content on the pure Al$_2$O$_3$ sample is low, whereas the significantly severe coke deposition formed on the Al$_2$O$_3$ support in the Pt/Sn-Al$_2$O$_3$ under the same conditions, and there are distinct differences in the weight loss temperatures. These results further confirm that the introduction of Pt enhances coke deposition on the alumina support due to the synergistic effect of the dehydrogenation function of Pt and the acidity of the alumina support.
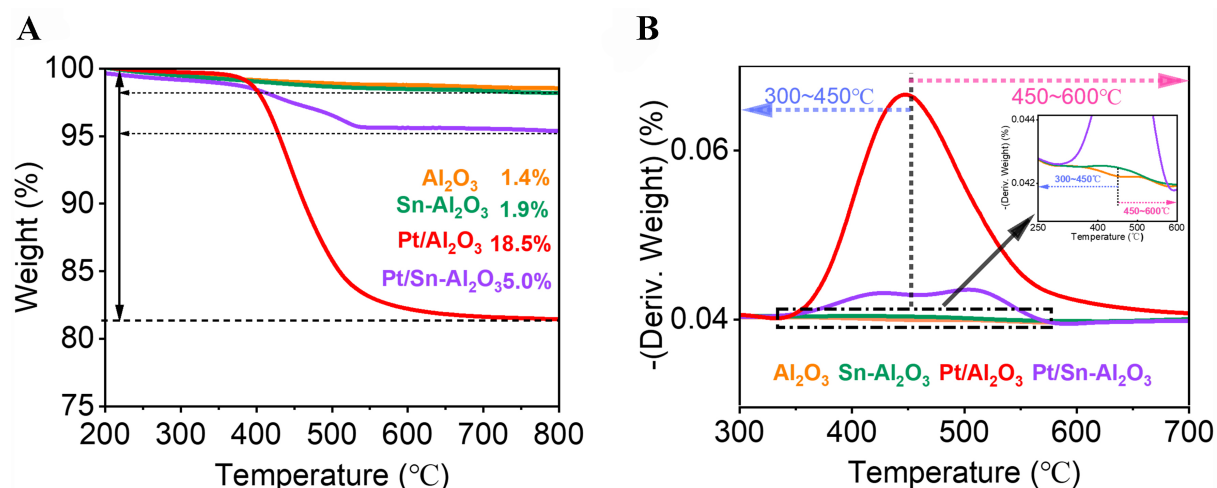
Figure 5. (A) TG profiles under air atmosphere and (B) corresponding DTG profiles of spent Al_2O_3, $Sn-Al_2O_3$, Pt/Al_2O_3 and $Pt/Sn-Al_2O_3$. The inset is the enlarged profiles at 250-600 °C. TG: Thermogravimetric; DTG: differential thermogravimetric.

The Raman spectroscopy was performed to further investigate the coke properties on various sites. Generally, the graphitic degree of coke can be reflected by the I_{D_1}/I_G ratio (height ratio of D1 and G bands), with a smaller value indicating a higher graphitic degree [Supplementary Figure 14][67]. The I_{D_1}/I_G ratios for Al_2O_3, $Sn-Al_2O_3$, Pt/Al_2O_3, $Pt/Sn-Al_2O_3$ after 3.3 h of reaction, and $Pt/Sn-Al_2O_3$ after 100 h of reaction are 0.96, 0.98, 0.71, 0.89, and 0.72, respectively. The I_{D_1}/I_G ratios for Al_2O_3 and $Sn-Al_2O_3$ are significantly higher than those for the Pt-based catalysts. In addition, the H/C (mol ratio) values from elemental analysis in Supplementary Table 4 show that Al_2O_3 (15.85) and $Sn-Al_2O_3$ (19.59) have higher H/C ratios than the Pt-based catalysts (< 3.96), indicating higher hydrogen content in coke species. This suggests less graphitic coke on Al_2O_3 and $Sn-Al_2O_3$ than Pt/Al_2O_3 and $Pt/Sn-Al_2O_3$.

Confocal fluorescence microscopy was employed to detect the non-graphitized coke on the catalyst after reactions [Supplementary Figure 15]. The significantly higher fluorescence intensity for Al_2O_3 and $Sn-Al_2O_3$ than Pt-based catalysts indicates their lower graphitic degree, which agrees with the Raman result. As shown in the confocal fluorescence spectrum [Supplementary Figure 15F], the peaks located at 421-481, 486-556, 561-646 and 651-736 nm are attributed to the benzene, naphthalene, anthracene and phenanthrene, benzophenanthrene and triphenylene, and coronene. The types of coke on Al_2O_3 and $Sn-Al_2O_3$ are similar. Interestingly, the $Sn-Al_2O_3$ sample has a higher content of benzene species than other samples, indicating that SnO_x sites are more prone to forming benzene species, which is consistent with the above FTIR results. The Pt/Al_2O_3 and $Pt/Sn-Al_2O_3$-100h samples did not show polycyclic coke species under fluorescence excitation, indicating that their coke species are mainly graphitized coke. These results suggest that the coke on Al_2O_3 and $Sn-Al_2O_3$ catalysts has a lower graphitic degree, compared with Pt-based catalysts.

To further explore the relationship between the Pt active phase, support acidity, and coke deposition on the support surface, Figure 6 presents the IR difference spectra after extensive isotope exchange reactions with H/D followed by pulsing with 500 Pa of propane for Al_2O_3 samples. As the reaction time increases, the intensity of the absorption peaks at 1,457-1,608 cm^{-1} gradually increases, indicating the formation of coke precursor species. Concurrently, the 2,400-2,800 cm^{-1} region, attributed to O–D stretching vibrations, shows a decreasing trend, while the 3,200-4,000 cm^{-1} region, corresponding to O–H stretching vibrations, tends to increase. This suggests that the O–D groups on the alumina support participate in the dehydrogenation of reactant molecules, leading to the formation of coke. Consequently, D atoms on the support surface are
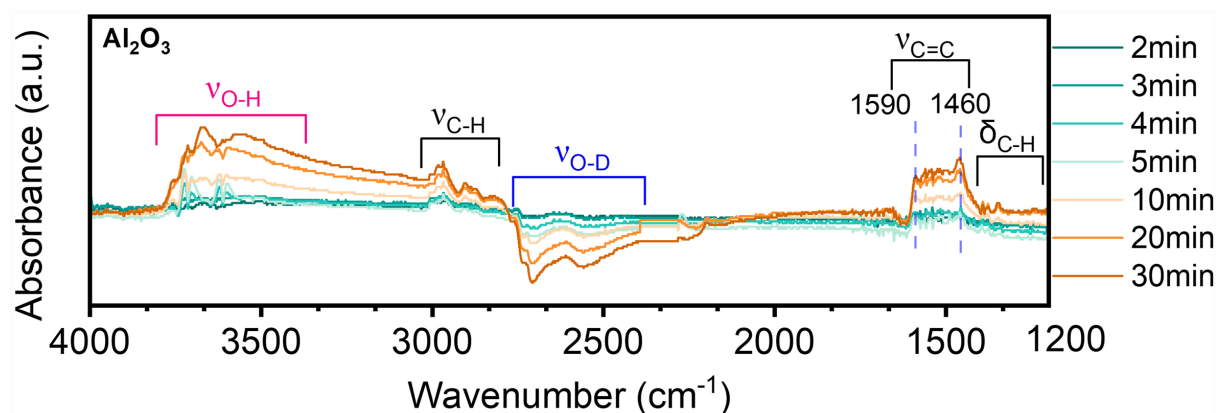
Figure 6. FTIR differential spectra following propane pulse adsorption for Al_2O_3 after D_2O replacement. The pulse experiments were carried out at 600 °C by pulses of pure propane (pulse volume = 0.50 cm³ STP) to the *in situ* cell at Ar (30 mL/min) atmosphere. FTIR: Fourier transform infrared spectroscopy; STP: standard temperature and pressure.

replaced by H, forming O–H. These data indicate that deep dehydrogenation and cyclization to form aromatic coke precursors occur on the Al_2O_3 surface, further confirming that the support contributes to the formation of coke precursors. In addition, the deactivation constant for the catalysts shows that the deactivation constant of Al_2O_3 is slightly higher than that of the catalysts containing Pt [Supplementary Table 5]. This indicates that the active sites on Al_2O_3 can accumulate coke, leading to catalyst deactivation.

The effect of hydrogen co-feed
It is well known that the introduction of H_2 can suppress the coke deposits in PDH. Therefore, we pulsed pure propane or C_3H_8/H_2 mixture (volume ratio = 1:1) (pulse volume = 0.50 cm³ STP) to the *in situ* cell under Ar flow (30 mL/min), and continuously recorded FTIR spectra for 5 min. Figure 7 presents a comparative FTIR difference spectrum of propane and a propane-hydrogen gas mixture, further exploring the impact of H_2 on the formation of coke precursor species on the Pt/Sn-Al_2O_3 catalyst. The absorption peaks attributed to aromatic hydrocarbons ν (C=C) in 1,470-1,600 cm⁻¹ show a significant decrease in intensity [Figure 7B and D], indicating that the introduction of H_2 effectively inhibits the formation of aromatic and unsaturated hydrocarbons. Additionally, an observation of the v_m (C–H) vibrational peak in the aromatic region of 3,050-3,140 cm⁻¹ further suggests that the aromatic species are dominated by a higher H/C ratio [Figure 7A and C]. The introduction of H_2 reduces the content and changes the types of coke precursor species.

In Supplementary Figure 16, *in-situ* FTIR spectra of CO adsorption were utilized to investigate the effect of feed composition on Pt sites. The area of the CO adsorption peak at Pt sites in the mixed-feed sample exhibits a lesser decline compared to the propane-only feed, indicating that the presence of H_2 inhibits the poisoning of Pt sites by coke deposition. In the mass spectrometry (MS) analysis presented in Figure 7C and D, a significant amount of propylene desorption is detected in the MS when C_3H_8 is fed alone, coupled with an increase in the intensity of the coke deposition IR peaks, suggesting that deep dehydrogenation on the catalyst leads to coke formation and poisons the Pt sites. Conversely, when the mixed feed is analyzed, a higher content of hydrogenolysis product CH_4 is detected, along with a decrease in the intensity of the coke IR peaks, indicating that the coke precursor species on the Pt sites undergo hydrogenolysis, thereby inhibiting the poisoning of Pt sites by coke. The introduction of hydrogen effectively controls and adjusts the content and types of coke precursor species while also preventing the poisoning of Pt sites by coke.
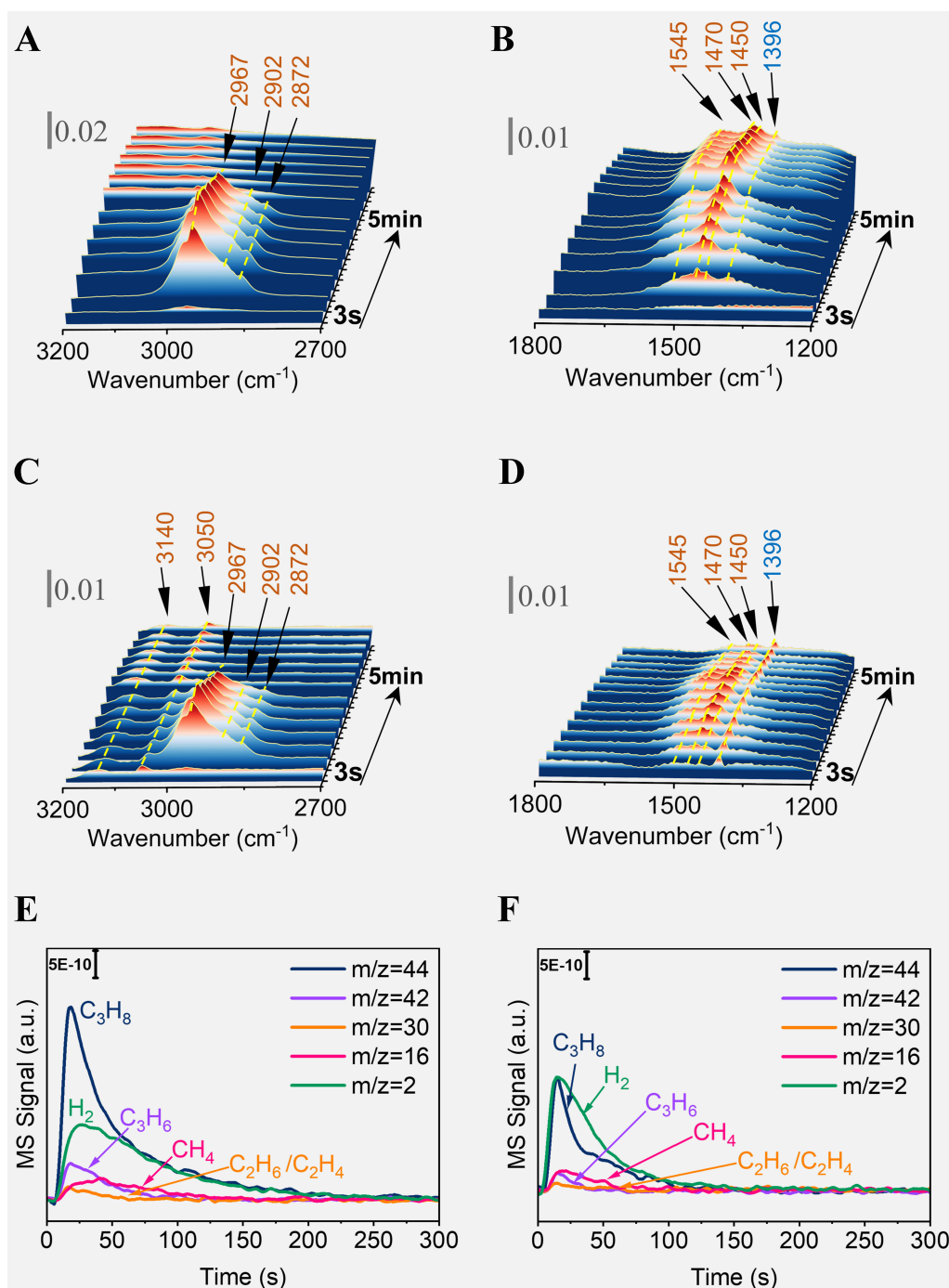
Figure 7. FTIR differential spectra following (A and B) pure C_3H_8 and (C and D) C_3H_8/H_2 mixture (volume ratio = 1:1) pulse adsorption for Pt/Sn-Al$_2$O$_3$, and corresponding mass spectrum of (E) pure C_3H_8 and (F) C_3H_8/H_2 mixture pulse. The pulse experiments were carried out at 600 °C by pulses of pure propane and C_3H_8/H_2 mixture (pulse volume = 0.50 cm^3 STP) to the *in situ* cell at Ar (30 mL/min) atmosphere. The yellow dashed line represents the adsorption peak. FTIR: Fourier transform infrared spectroscopy; STP: standard temperature and pressure.

CONCLUSIONS

The formation mechanisms of coke at Al$_2$O$_3$, Sn, Pt and Pt-Sn sites of Al$_2$O$_3$ supported PtSn catalysts in PDH are clarified. Compared to Pt and Pt-Sn sites, the coke initiation capability of Al$_2$O$_3$ and Sn is

significantly weaker. The tri-coordinated aluminum with Lewis acidity in Al_2O_3 is the primary site for coke formation, where propane undergoes excessive dehydrogenation to form propylidene and propylidyne, which further cyclize to form monocyclic and polycyclic aromatic coke precursors. The coke precursors at SnO_x sites differ from those on Al_2O_3, where the propyl species only forms monocyclic aromatic coke precursors after excessive dehydrogenation. For the Pt/Sn-Al_2O_3 catalyst, the strong dehydrogenation function and the interaction between Pt and supports trigger the complex coke formation mechanism. The coke formation is mainly ascribed to the following three factors: the structures of Pt-Sn clusters, active hydrogen species, Al_2O_3 support under the influence of active hydrogen species. The surface Pt sites with saturated coordination are prone to coke deposition, while the low-coordination Pt sites with ultra-small size are found to be highly resistant to coke formation in the PDH reaction. The strong dehydrogenation ability of Pt and the active hydrogen species play a vital role in the formation of coke precursors on Al_2O_3. Hydrogen co-feed also affects the formation of coke precursor. Hydrogen co-feed significantly inhibits the formation of coke precursors and leads to the formation of aromatic hydrocarbon coke precursors with higher H/C ratios. This work can provide the theoretical basis for the development of PDH catalysts with excellent coking resistance performance, and the established research method of coke is expected to be applied to more catalytic research fields.

DECLARATIONS

Authors' contributions
Designed, prepared and revised the manuscript: Jiao, J., Yang, Y., Song, L.
Discussion and preparation of the manuscript: Jiao, J., Yang, Y., Yuan, M., Tang, X., Shi, M., He, K., Zhang, H., Bi, Y., Qin, Y., Song, L.

Availability of data and materials
The detailed materials and methods in the experiment were listed in the Supplementary Materials. Other raw data that support the findings of this study are available from the corresponding author upon reasonable request.

Conflicts of interest
All authors declared that there are no conflicts of interest.

Ethical approval and consent to participate
Not applicable.

Consent for publication
Not applicable.

REFERENCES
1.   Song, S.; Yang, K.; Zhang, P.; et al. Silicalite-1 stabilizes Zn-hydride species for efficient propane dehydrogenation. *ACS. Catal.* **2022**, *12*, 5997-6006. DOI

2. Hou, W.; Lin, K.; Zhang, X.; et al. Highly stable and selective Pt/TS-1 catalysts for the efficient nonoxidative dehydrogenation of propane. *Chem. Eng. J.* **2023**, *474*, 145648. DOI

3. Festa, G.; Contaldo, P.; Martino, M.; Meloni, E.; Palma, V. Modeling the selectivity of hydrotalcite-based catalyst in the propane dehydrogenation reaction. *Ind. Eng. Chem. Res.* **2023**, *62*, 16622-37. DOI PubMed PMC

4. Phadke, N. M.; Mansoor, E.; Bondil, M.; Head-Gordon, M.; Bell, A. T. Mechanism and kinetics of propane dehydrogenation and cracking over Ga/H-MFI prepared via vapor-phase exchange of H-MFI with $GaCl_3$. *J. Am. Chem. Soc.* **2019**, *141*, 1614-27. DOI PubMed

5. Nakaya, Y.; Hirayama, J.; Yamazoe, S.; Shimizu, K. I.; Furukawa, S. Single-atom Pt in intermetallics as an ultrastable and selective catalyst for propane dehydrogenation. *Nat. Commun.* **2020**, *11*, 2838. DOI PubMed PMC

6. Ma, Y.; Chen, X.; Guan, Y.; et al. Skeleton-Sn anchoring isolated Pt site to confine subnanometric clusters within *BEA topology. *J. Catal.* **2021**, *397*, 44-57. DOI

7. Shi, L.; Deng, G. M.; Li, W. C.; et al. Al_2O_3 nanosheets rich in pentacoordinate Al^{3+} ions stabilize Pt-Sn clusters for propane dehydrogenation. *Angew. Chem. Int. Ed. Engl.* **2015**, *54*, 13994-8. DOI PubMed

8. Ma, Y.; Song, S.; Liu, C.; et al. Germanium-enriched double-four-membered-ring units inducing zeolite-confined subnanometric Pt clusters for efficient propane dehydrogenation. *Nat. Catal.* **2023**, *6*, 506-18. DOI

9. Wei, S.; Dai, H.; Long, J.; et al. Nonoxidative propane dehydrogenation by isolated Co^{2+} in BEA zeolite: dealumination-determined key steps of propane C–H activation and propylene desorption. *Chem. Eng. J.* **2023**, *455*, 140726. DOI

10. Wan, H.; Qian, L.; Gong, N.; et al. Size-dependent structures and catalytic properties of supported bimetallic PtSn catalysts for propane dehydrogenation reaction. *ACS. Catal.* **2023**, *13*, 7383-94. DOI

11. Wang, P.; Senftle, T. P. Modeling phase formation on catalyst surfaces: coke formation and suppression in hydrocarbon environments. *AIChE. J.* **2021**, *67*, e17454. DOI

12. Zhang, Y.; Aly, M. Effect of CO_2 on activity and coke formation over gallium-based catalysts for propane dehydrogenation. *Appl. Catal. A. Gen.* **2022**, *643*, 118795. DOI

13. Sun, M.; Hu, Z.; Wang, H.; Suo, Y.; Yuan, Z. Design strategies of stable catalysts for propane dehydrogenation to propylene. *ACS. Catal.* **2023**, *13*, 4719-41. DOI

14. Chen, S.; Chang, X.; Sun, G.; et al. Propane dehydrogenation: catalyst development, new chemistry, and emerging technologies. *Chem. Soc. Rev.* **2021**, *50*, 3315-54. DOI PubMed

15. Xiao, L.; Shan, Y.; Sui, Z.; et al. Beyond the reverse Horiuti–Polanyi mechanism in propane dehydrogenation over Pt catalysts. *ACS. Catal.* **2020**, *10*, 14887-902. DOI

16. Xiong, H.; Lin, S.; Goetze, J.; et al. Thermally stable and regenerable platinum–tin clusters for propane dehydrogenation prepared by atom trapping on ceria. *Angew. Chem.* **2017**, *129*, 9114-9. DOI

17. Zhang, W.; Wang, H.; Jiang, J.; et al. Size dependence of Pt catalysts for propane dehydrogenation: from atomically dispersed to nanoparticles. *ACS. Catal.* **2020**, *10*, 12932-42. DOI

18. Gao, X.; Yao, Z.; Li, W.; et al. Calcium-modified $PtSn/Al_2O_3$ catalyst for propane dehydrogenation with high activity and stability. *ChemCatChem* **2023**, *15*, e202201691. DOI

19. Yu, Q.; Yu, T.; Chen, H.; Fang, G.; Pan, X.; Bao, X. The effect of Al^{3+} coordination structure on the propane dehydrogenation activity of $Pt/Ga/Al_2O_3$ catalysts. *J. Energy. Chem.* **2020**, *41*, 93-9. DOI

20. Kwak, J. H.; Hu, J.; Mei, D.; et al. Coordinatively unsaturated Al^{3+} centers as binding sites for active catalyst phases of platinum on gamma-Al_2O_3. *Science* **2009**, *325*, 1670-3. DOI PubMed

21. Li, X.; Li, J.; Yuan, M.; et al. Effect of chlorine on the performance of Cr-K/γ-Al_2O_3 catalyst for *n*-hexane dehydrogenation. *Appl. Catal. A. Gen.* **2023**, *664*, 119322. DOI

22. Sun, G.; Zhao, Z. J.; Li, L.; et al. Metastable gallium hydride mediates propane dehydrogenation on H_2 co-feeding. *Nat. Chem.* **2024**, *16*, 575-83. DOI PubMed

23. Wang, Z.; Chen, Y.; Mao, S.; et al. Chemical insight into the structure and formation of coke on PtSn alloy during propane dehydrogenation. *Adv. Sustain. Syst.* **2020**, *4*, 2000092. DOI

24. Zhao, Z. J.; Wu, T.; Xiong, C.; et al. Hydroxyl-mediated non-oxidative propane dehydrogenation over VO_x/γ-Al_2O_3 catalysts with improved stability. *Angew. Chem. Int. Ed. Engl.* **2018**, *57*, 6791-5. DOI PubMed

25. Sun, G.; Zhao, Z. J.; Mu, R.; et al. Breaking the scaling relationship via thermally stable Pt/Cu single atom alloys for catalytic dehydrogenation. *Nat. Commun.* **2018**, *9*, 4454. DOI PubMed PMC

26. Biloen, P. Catalytic dehydrogenation of propane to propene over platinum and platinum-gold alloys. *J. Catal.* **1977**, *50*, 77-86. DOI

27. Sattler, J. J.; Ruiz-Martinez, J.; Santillan-Jimenez, E.; Weckhuysen, B. M. Catalytic dehydrogenation of light alkanes on metals and metal oxides. *Chem. Rev.* **2014**, *114*, 10613-53. DOI PubMed

28. Yuan, Y.; Brady, C.; Lobo, R. F.; Xu, B. Understanding the correlation between Ga speciation and propane dehydrogenation activity on Ga/H-ZSM-5 catalysts. *ACS. Catal.* **2021**, *11*, 10647-59. DOI

29. Phadke, N. M.; Mansoor, E.; Head-gordon, M.; Bell, A. T. Mechanism and kinetics of light alkane dehydrogenation and cracking over isolated Ga species in Ga/H-MFI. *ACS. Catal.* **2021**, *11*, 2062-75. DOI

30. Li, M.; Yin, W.; Pan, J.; et al. Hydrogen spillover as a promising strategy for boosting heterogeneous catalysis and hydrogen storage. *Chem. Eng. J.* **2023**, *471*, 144691. DOI

31. Niu, X.; Zhao, R.; Han, Y.; Zhang, X.; Wang, Q. Highly dispersed platinum clusters anchored on hollow ZSM-5 zeolite for deep

hydrogenation of polycyclic aromatic hydrocarbons. *Fuel* **2022**, *326*, 125021. DOI

32. Wang, G.; Li, C.; Shan, H. Catalytic dehydrogenation of isobutane over a Ga$_2$O$_3$/ZnO interface: reaction routes and mechanism. *Catal. Sci. Technol.* **2016**, *6*, 3128-36. DOI

33. Dewangan, N.; Ashok, J.; Sethia, M.; et al. Cobalt-based catalyst supported on different morphologies of alumina for non-oxidative propane dehydrogenation: effect of metal support interaction and lewis acidic sites. *ChemCatChem* **2019**, *11*, 4923-34. DOI

34. Soma, Y. Infrared spectra of ethylene adsorbed on transition metals at low temperatures and hydrogenation of the adsorbed species. *J. Catal.* **1979**, *59*, 239-47. DOI

35. Ko, M. K.; Frei, H. Millisecond FT-IR spectroscopy of surface intermediates of C$_2$H$_4$ hydrogenation over Pt/Al$_2$O$_3$ catalyst under reaction conditions. *J. Phys. Chem. B.* **2004**, *108*, 1805-8. DOI

36. Arena, F.; Dario, R.; Parmaliana, A. A characterization study of the surface acidity of solid catalysts by temperature programmed methods. *Appl. Catal. A.* **1998**, *170*, 127-37. DOI

37. Buzzoni, R.; Bordiga, S.; Ricchiardi, G.; Lamberti, C.; Zecchina, A.; Bellussi, G. Interaction of pyridine with acidic (H-ZSM5, H-β, H-MORD zeolites) and superacidic (H-nafion membrane) systems: an IR investigation. *Langmuir* **1996**, *12*, 930-40. DOI

38. Cholewinski, M. C.; Dixit, M.; Mpourmpakis, G. Computational study of methane activation on γ-Al$_2$O$_3$. *ACS. Omega.* **2018**, *3*, 18242-50. DOI PubMed PMC

39. Dixit, M.; Kostetskyy, P.; Mpourmpakis, G. Structure–activity relationships in alkane dehydrogenation on γ-Al$_2$O$_3$: site-dependent reactions. *ACS. Catal.* **2018**, *8*, 11570-8. DOI

40. Otroshchenko, T.; Sokolov, S.; Stoyanova, M.; et al. ZrO$_2$-based alternatives to conventional propane dehydrogenation catalysts: active sites, design, and performance. *Angew. Chem. Int. Ed. Engl.* **2015**, *54*, 15880-3. DOI PubMed

41. Li, C.; Guo, X.; Shang, Q.; et al. Defective TiO$_2$ for propane dehydrogenation. *Ind. Eng. Chem. Res.* **2020**, *59*, 4377-87. DOI

42. Wang, P.; Xu, Z.; Wang, T.; Yue, Y.; Bao, X.; Zhu, H. Unmodified bulk alumina as an efficient catalyst for propane dehydrogenation. *Catal. Sci. Technol.* **2020**, *10*, 3537-41. DOI

43. Leclerc, H.; Vimont, A.; Lavalley, J. C.; et al. Infrared study of the influence of reducible iron(III) metal sites on the adsorption of CO, CO$_2$, propane, propene and propyne in the mesoporous metal-organic framework MIL-100. *Phys. Chem. Chem. Phys.* **2011**, *13*, 11748-56. DOI PubMed

44. Čapek, L.; Novoveská, K.; Sobalík, Z.; Wichterlová, B.; Cider, L.; Jobson, E. Cu-ZSM-5 zeolite highly active in reduction of NO with decane under water vapor presence. *Appl. Catal. B. Environ.* **2005**, *60*, 201-10. DOI

45. Hadjiivanov, K. Chapter two - Identification and characterization of surface hydroxyl groups by infrared spectroscopy. *Adv. Catal.* **2014**, *57*, 99-318. DOI

46. Vazhnova, T.; Rigby, S. P.; Lukyanov, D. B. Benzene alkylation with ethane in ethylbenzene over a PtH-MFI catalyst: kinetic and IR investigation of the catalyst deactivation. *J. Catal.* **2013**, *301*, 125-33. DOI

47. Madeira, F. F.; Vezin, H.; Gnep, N. S.; Magnoux, P.; Maury, S.; Cadran, N. Radical species detection and their nature evolution with catalyst deactivation in the ethanol-to-hydrocarbon reaction over HZSM-5 zeolite. *ACS. Catal.* **2011**, *1*, 417-24. DOI

48. Song, C.; Liu, K.; Zhang, D.; et al. Effect of cofeeding n-butane with methanol on aromatization performance and coke formation over a Zn loaded ZSM-5/ZSM-11 zeolite. *Appl. Catal. A. Gen.* **2014**, *470*, 15-23. DOI

49. Roy, S.; Bakhmutsky, K.; Mahmoud, E.; Lobo, R. F.; Gorte, R. J. Probing lewis acid sites in Sn-beta zeolite. *ACS. Catal.* **2013**, *3*, 573-80. DOI

50. Zhu, Y.; An, Z.; Song, H.; Xiang, X.; Yan, W.; He, J. Lattice-confined Sn (IV/II) stabilizing raft-like Pt clusters: high selectivity and durability in propane dehydrogenation. *ACS. Catal.* **2017**, *7*, 6973-8. DOI

51. Wang, F.; Xiao, W.; Gao, L.; Xiao, G. Enhanced performance of glycerol to aromatics over Sn-containing HZSM-5 zeolites. *RSC. Adv.* **2016**, *6*, 42984-93. DOI

52. Karge, H.; Nießen, W.; Bludau, H. In-situ FTIR measurements of diffusion in coking zeolite catalysts. *Appl. Catal. A. Gen.* **1996**, *146*, 339-49. DOI

53. Wong, K. S.; Vazhnova, T.; Rigby, S. P.; Lukyanov, D. B. Temperature effects in benzene alkylation with ethane into ethylbenzene over a PtH-MFI bifunctional catalyst. *Appl. Catal. A. Gen.* **2013**, *454*, 137-44. DOI

54. van den Brand J, Blajiev O, Beentjes PC, Terryn H, de Wit JH. Interaction of ester functional groups with aluminum oxide surfaces studied using infrared reflection absorption spectroscopy. *Langmuir* **2004**, *20*, 6318-26. DOI PubMed

55. Zaki, M. I.; Hasan, M. A.; Al-sagheer, F. A.; Pasupulety, L. Surface chemistry of acetone on metal oxides: IR observation of acetone adsorption and consequent surface reactions on silica−alumina versus silica and alumina. *Langmuir* **2000**, *16*, 430-6. DOI

56. Airaksinen, S.; Banares, M.; Krause, A. In situ characterisation of carbon-containing species formed on chromia/alumina during propane dehydrogenation. *J. Catal.* **2005**, *230*, 507-13. DOI

57. Finocchio, E.; Busca, G.; Lorenzelli, V.; Willey, R. The activation of hydrocarbon CH bonds over transition metal oxide catalysts: a FTIR study of hydrocarbon catalytic combustion over MgCr$_2$O$_4$. *J. Catal.* **1995**, *151*, 204-15. DOI

58. Deng, X.; Qin, B.; Liu, R.; et al. Zeolite-encaged isolated platinum ions enable heterolytic dihydrogen activation and selective hydrogenations. *J. Am. Chem. Soc.* **2021**, *143*, 20898-906. DOI PubMed

59. Pei, Y.; Qi, Z.; Goh, T. W.; et al. Intermetallic structures with atomic precision for selective hydrogenation of nitroarenes. *J. Catal.* **2017**, *356*, 307-14. DOI

60. Vaarkamp, M.; Miller, J. T.; Modica, F. S.; Koningsberger, D. C. On the relation between particle morphology, structure of the metal-support interface, and catalytic properties of Pt/γ-Al$_2$O$_3$. *J. Catal.* **1996**, *163*, 294-305. DOI

61. Bazin, P.; Saur, O.; Lavalley, J. C.; Daturi, M.; Blanchard, G. FT-IR study of CO adsorption on Pt/CeO$_2$: characterisation and structural rearrangement of small Pt particles. *Phys. Chem. Chem. Phys.* **2005**, *7*, 187. DOI

62. Liu, L.; Lopez-haro, M.; Lopes, C. W.; et al. Structural modulation and direct measurement of subnanometric bimetallic PtSn clusters confined in zeolites. *Nat. Catal.* **2020**, *3*, 628-38. DOI

63. Han, L.; Meng, Q.; Wang, D.; et al. Interrogation of bimetallic particle oxidation in three dimensions at the nanoscale. *Nat. Commun.* **2016**, *7*, 13335. DOI PubMed PMC

64. Kim, T.; Kim, J.; Song, H. C.; et al. Catalytic synergy on PtNi bimetal catalysts driven by interfacial intermediate structures. *ACS. Catal.* **2020**, *10*, 10459-67. DOI

65. Wang, C. M.; Schreiber, D. K.; Olszta, M. J.; Baer, D. R.; Bruemmer, S. M. Direct in Situ TEM observation of modification of oxidation by the injected vacancies for Ni-4Al alloy using a microfabricated nanopost. *ACS. Appl. Mater. Interfaces.* **2015**, *7*, 17272-7. DOI PubMed

66. Allian, A. D.; Takanabe, K.; Fujdala, K. L.; et al. Chemisorption of CO and mechanism of CO oxidation on supported platinum nanoclusters. *J. Am. Chem. Soc.* **2011**, *133*, 4498-517. DOI PubMed

67. Liu, J.; Zhao, Z.; Xu, C.; et al. In-situ UV-Raman study on soot combustion over TiO$_2$ or ZrO$_2$-supported vanadium oxide catalysts. *Sci. China. Ser. B. Chem.* **2008**, *51*, 551-61. DOI

Jianhao Jiao obtained his M.S. degree in Chemical Engineering from Liaoning Petrochemical University in 2020. In the same year, he began his Ph.D. studies in Chemical Engineering and Technology at China University of Petroleum (East China) under the supervision of Prof. Lijuan Song. His research focuses on the identification and construction of active sites of Pt-based propane dehydrogenation catalysts and the establishment of structure-activity relationships.

Jianhao Jiao

Ye Yang obtained his Ph.D. from China University of Petroleum (East China) under the supervision of Prof. Xinmei Liu in 2022. He then joined Prof. Lijuan Song's group at Liaoning Petrochemical University as a lecturer. His research interests mainly center on the transformation and utilization of light hydrocarbons, green catalytic materials and processes, and the synthesis of metal/zeolite bifunctional catalysts.

Ye Yang

Maojie Yuan

Maojie Yuan earned his B.S. degree at Yangtze Normal University in 2022 and, in the same year, embarked on his M.S. studies under the supervision of Prof. Lijuan Song at Liaoning Petrochemical University. His research delves into the design and preparation of potassium-modified $PtSn/Al_2O_3$ catalysts for propane dehydrogenation.

Xuqi Tang

Xuqi Tang completed his B.S. degree in Chemistry from Qujing Normal University in 2022 and subsequently advanced to M.S. studies at Liaoning Petrochemical University. His research pursuits involve the identification of active sites of Pt-based propane dehydrogenation catalysts.

Mengfan Shi

Mengfan Shi graduated with a B.S. degree in Chemistry from Hebei Normal University for Nationalities in 2023. She then pursued her M.S. under the supervision of Prof. Lijuan Song at Liaoning Petrochemical University. Her research currently explores the effect of platinum sources on the active site and catalytic performance of Pt-based propane dehydrogenation catalysts.

Kai He

Kai He received his B.S. degree in Chemical Engineering and Technology from Liaocheng University in 2018, followed by an M.S. in Chemical Technology at Liaoning Petrochemical University under Prof. Yanfeng Bi's guidance in 2022. Currently a Ph.D. candidate under the supervision of Prof. Lijuan Song at China University of Petroleum (East China), his research investigates the theoretical study of surface active site construction of metal oxides.

Haijuan Zhang

Haijuan Zhang obtained her Ph.D. from Tianjin University (China) in 2006 and subsequently conducted industrial applied research at the Fushun Research Institute of Petroleum and Petrochemicals, SINOPEC, from 2006 to 2015. She joined the faculty of Liaoning Petrochemical University in 2015 and has held the position of full professor since 2020. Her primary research interests lie in the comprehensive utilization of light hydrocarbons, especially propane dehydrogenation. She is also dedicated to advancing the fundamental understanding of hydrodesulfurization catalysts.

Yanfeng Bi

Yanfeng Bi obtained his Ph.D. from the Changchun Institute of Applied Chemistry (CIAC), Chinese Academy of Science (CAS), in 2011. He then worked at the State Key Laboratory of Rare Earth Resource Utilization of CIAC from 2011 to 2014. In 2015, he joined Liaoning Petrochemical University, where he currently serves as a professor in the School of Petrochemical Engineering. His current research focuses on the synthesis and applications of metal nanoclusters.

Yucai Qin obtained his Ph.D. from China University of Petroleum (East China) in 2014 and began his teaching career at Liaoning Petrochemical University. He has been a full professor at the university since 2022 and is now the associate dean of the College of Petrochemical Engineering. His research interests focus on the development of green catalysis and separation science and technology for zeolites in the fields of petrochemicals and fine chemicals.

Yucai Qin

Lijuan Song received her first Degree in Chemical Engineering from Tianjin University in 1984. In 2000, she completed her Ph.D. in Physical Chemistry at the University of Edinburgh, UK, under the supervision of Prof. Lovat Rees. She continued her collaboration with Prof. Rees as a postdoc research fellow until the end of 2004 when she rejoined Liaoning Petrochemical University. She has been a professor at the university since then and is now the director of the Key Laboratory of Petrochemical Catalysis Science and Technology, Liaoning Province. She has been awarded a Distinguished Professor in the province and a State Council Government Special Allowance Expert in China. Her research interests mainly lie in the adsorption and diffusion in porous materials, the transformation and utilization of light hydrocarbons, green catalytic materials and processes, clean fuels, *etc.*

Lijuan Song